Forced hydrolysis of $FeCl_3$ solutions in the presence of Cr^{3+} ions and hexamethylenetetramine

Marko Robić[1, a)], Mira Ristić[1], Stjepko Krehula[1], Ernő Kuzmann[2], Zoltán Homonnay[2], Svetozar Musić[1,3]

[1] *Division of Materials Chemistry, Ruđer Bošković Institute, P.O.Box 180, HR-10002, Zagreb, Croatia*

[2] *Institute of Chemistry, Eötvös Loránd University, Budapest, Hungary*

[3] *Croatian Academy of Sciences and Arts, Nikola Šubić Zrinski Square 11, HR-10000 Zagreb, Croatia*

[a)] Address all correspondence to this author. E-mail: mrobic@irb.hr

Abstract

The phase analysis and nanostructural properties of the precipitates formed by forced hydrolysis of $FeCl_3$ solutions at 160 °C in the presence of Cr^{3+} ions and hexamethylenetetramine (HMTA) were investigated. The phase analyses of the precipitates showed the presence of ferrihydrite (amorphous-like), α-FeOOH, β-FeOOH and α-Fe_2O_3. The exact phase composition was strongly dependent on the starting chemical composition in the solution and the precipitation time. Ferrihydrite, α-FeOOH and β-FeOOH were the precursors of α-Fe_2O_3 as the end-product. Upon 2 h of autoclaving at 160 °C the precipitates consisted of nanoparticles ~35 to ~50 nm in size, whereas after 24 h their size increased to ~100 nm. New shapes of these nanoparticles were found. In these precipitation systems crystalline chromium (hydrous)oxide phase was not detected. However, the formation of solid solutions between Cr^{3+} ions and iron oxides could not be excluded taking into account Energy-dispersive X-ray spectroscopy (EDS) measurements.

Keywords

Fe, Cr, kinetics, morphology, Mössbauer effect, oxide

---

*This work was presented at the ACS Fall National Meeting, Atlanta, Georgia, USA, August 22-26 2021

Introduction

Precipitation of iron oxides (group name for iron-hydroxides, -oxyhydroxides and –oxides) was the subject of many investigations [1,2]. The simplest way to precipitate iron oxides is a slow or forced hydrolysis of Fe(III) salt solutions. Precipitation of iron oxides from mixed Fe(II)/Fe(III)-salt solutions by adding an alkali was also the subject of investigations. These precipitation processes are influenced by various additions such as metal cations, oxyanions, surfactants and polymers, as well as solvents. In such way it is possible to change or enhance some specific properties of iron oxides.

Generally, in these precipitation processes the mixtures of various iron oxides are forming with different nanostructures. Hydrolysis of hexamethylenetetramine (HMTA) at elevated temperature was also used in the investigation of the precipitation of iron oxides from aqueous solutions. Musić et al. [3] and Šarić et al. [4,5] investigated the phase composition and microstructural properties of iron oxides precipitated in the presence of decomposing HMTA. Precipitation of some other metal oxides in the presence of decomposing HMTA was also investigated. Dolgopolova et al. [6] utilized decomposing HMTA in the preparation of Gd-doped CeO_2, whereas Wang et al. [7] and Anas et al. [8] investigated changes in ZnO morphology and functional properties. Nanosized MgO particles prepared from Mg-acetate and HMTA solution showed a good removal of arsenates and phosphates from waste solutions [9]. An internal-gelation process for the preparation of UO_2 microspheres was developed by using HMTA decomposition [10].

HMTA undergoes homogenous hydrolysis in the water medium at elevated temperature in line with chemical reactions:

$$C_6H_{12}N_4 + 6H_2O \rightarrow 6HCHO + 4NH_3 \quad (1)$$

and

$$NH_3 + H_2O \rightarrow NH_4^+ + OH^- \quad (2)$$

A gradual release of OH^- ions increases the pH in the solution and the corresponding kinetics is temperature dependent.

The addition of HMTA also made it possible to extend the pH region of the homogenous Fe^{3+} hydrolysis, as well as to eliminate the problems that could occur upon an abrupt addition of the NaOH or NH_4OH solution to the system (heterogeneous precipitation). Even in the case of a controlled addition of the NaOH or NH_4OH solution,

it is impossible to obtain conditions like those with HMTA. Finally, the time of aging of the precipitation systems was long enough to observe the tendencies in the phase transformation of the precipitates.

Besides that, formaldehyde is generated in the autoclaving system at elevated temperatures as a by-product. According to the presented equation, formaldehyde is generated in a ratio of 6:4 relative to ammonia, which means that a large amount of formaldehyde is present in the autoclaving system. Consequently, $FeCl_3$ is then actually dissolved in the mixture of water and formaldehyde. As a solvent, this mixture has different properties than pure water. Considering that, formaldehyde's influence on the structure of the products cannot be excluded.

In continuation to our previous works [3-5] we are now reporting new results concerning precipitation from $FeCl_3$ solutions containing Cr^{3+} ions and decomposing HMTA. Combining X-ray powder diffraction (XRD), ^{57}Fe Mössbauer spectroscopy, Fourier-transform infrared spectroscopy (FT-IR), Field Emission Scanning Electron Microscopy (FE SEM) and Energy-dispersive X-ray spectroscopy (EDS) made it possible to monitor changes in the phase composition and nanostructure of the solid phase obtained, with a view of better understanding the processes in the precipitation systems investigated.

The present investigation is not important only from the academic standpoint, but also for a better understanding of different processes, such as aqueous and atmospheric corrosion of steel, catalysis and photocatalysis, the role of Cr-doped electrode material for Li-ion batteries or decontamination of polluted waters with iron oxides.

Results and discussion

X-ray powder diffraction

XRD analyses of samples M1 through M16 showed the effect of HMTA on the phase composition of the precipitates. The XRD patterns of all synthesized samples are summarized in Figures 1 and 2, while the results of phase identifications by XRD and ^{57}Fe Mössbauer measurements are given in Table 1. Forced hydrolysis of the 0.1M $FeCl_3$ solution in the presence of 0.25M HMTA between 2 and 24 h showed a set of phase transformations. Upon 2 h of forced hydrolysis the formed precipitate contained a mixture of α-Fe_2O_3, α-FeOOH and ferrihydrite (sample M1). Upon a prolonged autoclaving time

the ferrihydrite component disappeared, whereas α-Fe_2O_3 and α-FeOOH remained (samples M2 and M3). Upon 24 h of autoclaving α-Fe_2O_3 was found as a single phase (sample M4). Forced hydrolysis of 0.2M $FeCl_3$ solution in decomposing HMTA upon 2 h (sample M5) yielded predominantly β-FeOOH and small amounts of α-Fe_2O_3/α-FeOOH. Samples M6, M7 and M8 showed the presence of α-Fe_2O_3 and α-FeOOH phases. Samples M9 through M12 were prepared by forced hydrolysis of the 0.09M $FeCl_3$ + 0.01M $CrCl_3$ solution. Upon 2 h of autoclaving sample M9 consisted of ferrihydrite and a small fraction of α-Fe_2O_3. Samples M10, M11 and M12 contained mixtures of α-Fe_2O_3 and α-FeOOH. β-FeOOH as a single phase was prepared upon 2 h of autoclaving the 0.18M $FeCl_3$ + 0.02M $CrCl_3$ solution (sample M13), whereas mixtures of β-FeOOH and α-Fe_2O_3 were produced by autoclaving up to 24 h (samples M14, M15, M16). In a previous work [11] we have found that precipitation from the $CrCl_3$ solution (no added $FeCl_3$) in the presence of HMTA under similar conditions yielded nanosize α-CrOOH (grimaldiite) as a single phase. However, in samples M1 through M16 no grimaldiite or any crystalline hydrous chromium oxide phase was found. It is known that Cr^{3+} ions practically do not form hydroxyl complexes up to pH~4, then with a further pH increase an abrupt hydrolysis of Cr^{3+} ions occurs [12]. However, the incorporation of Cr^{3+} ions into Fe-oxide phases in the form of solid solutions cannot be eliminated, since the pH_{final} values (see Experimental, Table 2) are in the range where Cr^{3+} ions are well hydrolyzed. This conclusion is also corroborated by close ionic radii of Fe^{3+} (64.5 pm) and Cr^{3+} (61.5 pm) [13].

^{57}Fe Mössbauer spectroscopy

Figures 3A and 4A show the Mössbauer spectra of samples M1 through M16, while the calculated Mössbauer parameters are given in Table 3. The spectrum of sample M1 is considered a superposition of one central quadrupole doublet with broadened spectral lines and two hyperfine magnetic field (B_{hf}) components. In line with XRD results this central quadrupole doublet can be assigned to the presence of ferrihydrite. Two hyperfine magnetic fields are due to the presence of α-Fe_2O_3 and α-FeOOH phases. Lower B_{hf} values can be generally attributed to the reduced crystallinity and/or the presence of fine particles in these two phases. Samples M2 and M3 correspond to the presence of α-

Fe_2O_3 and α-FeOOH, whereas sample M4 corresponds to α-Fe_2O_3 as a single phase. The spectrum of sample M5 is considered the superposition of two quadrupole doublets corresponding to β-FeOOH and one B_{hf} component of small relative intensity corresponding to α-Fe_2O_3 traces. Mössbauer spectra of samples M6 through M8 showed the superposition of two sextets corresponding to α-Fe_2O_3 and α-FeOOH phases, and upon prolonged autoclaving time the α-FeOOH amount decreased. The spectrum of sample M9 (Figure 4A) is considered a superposition of the dominant central quadrupole doublet, which in line with XRD measurements can be assigned to 2-XRD lines ferrihydrite, and a sextet of small relative intensity which can be assigned to the presence of the α-Fe_2O_3 phase. Ristić et al. [14] reported the development of the Mössbauer spectrum of 2-XRD lines ferrihydrite between RT and 12 K giving also the corresponding Mössbauer parameters. Within only 2 hours of autoclaving, 2-XRD lines ferrihydrite content is decreasing drastically from 92.00 % in sample M9 to 21.70 % in sample M10 (see Table 3). This data indicates that transformation from 2-XRD lines ferrihydrite to α-Fe_2O_3 phase is a very fast process in the first 2 hours. Reference samples series M1-M4 (autoclaved without Cr^{3+}) compared to M9-M12 (autoclaved with Cr^{3+}) are showing much faster disappearance of 2-XRD lines ferrihydrite. From this data, it can be concluded that the system with Cr^{3+} shows inhibition of transformation of 2-XRD lines ferrihydrite to α-Fe_2O_3 phase. When Cr^{3+} is present in the autoclaving solution, 2-XRD lines ferrihydrite doesn't completely disappear (samples M9-M12). The spectra additionally show a slight increase in α-FeOOH phase from 11.57 % (sample M10) to 15.62 % (sample M12). The spectrum of sample M13 is resolved into two central quadrupole doublets with parameters corresponding to β-FeOOH, whereas the spectra of samples M14 to M16 showed a larger amount of the α-Fe_2O_3 phase with a corresponding decrease in the β-FeOOH phase. The most pronounced decrease of β-FeOOH phase is observable from sample M15 (6 h of autoclaving) to sample M16 (24 h of autoclaving), which points out that the transformation of β-FeOOH into α-Fe_2O_3 is a slow process within this sample series (M13-M16). Reference sample series (M5-M8) prepared without chromium behave differently since β-FeOOH is present only within the first 2 h of autoclaving (M5) and then it completely disappears even after only 4 h of autoclaving (sample M6). This indicates that within the

reference sample series (M5-M8) β-FeOOH transforms relatively fast (compared to series M13-M16 autoclaved with Cr^{3+}). So, it can be concluded that Cr^{3+} shows inhibiting effect in both sample series (M9-M12 and M13-M16), regardless of whether it is transformation from 2-XRD lines ferrihydrite or β-FeOOH to α-Fe_2O_3.

Fourier-transform infrared spectroscopy

The results of FT-IR spectroscopic measurements are summarized in Figures 3B and 4B. Samples M1 to M3 showed the presence of α-FeOOH and α-Fe_2O_3, whereas the spectrum of sample M4 showed the presence of α-Fe_2O_3 as a single phase. Two prominent IR bands typical of the α-FeOOH phase at 801 to 811 cm^{-1} and 896 to 899 cm^{-1} were assigned to Fe-O-H bending vibrations (δ_{OH} and σ_{OH}, respectively) [15]. The FT-IR spectrum of sample M4 is characterized by three IR bands at 514, 428 and 382 cm^{-1} and two shoulders at 566 and 464 cm^{-1}. Generally, the FT-IR spectrum of α-Fe_2O_3 shows six active vibrations, two A_{2u} (EIIc) and four E_u ($E\perp c$). The shape of the IR spectrum of α-Fe_2O_3 is sensitive to the degree of its crystallinity as well as the size, shape and aggregation of the particles [16]. Wang et al. [17] also reported a broadening of IR bands at the reduced size of subcrystals in α-Fe_2O_3 particles. The FT-IR spectrum of sample M5 is characterized by very broad lines at 697 and 629 cm^{-1}, which can be identified due to the presence of β-FeOOH while taking into account the results of XRD and Mössbauer measurements. Very broad IR bands observed for sample M5 can be assigned to the presence of very fine β-FeOOH particles in the nanosize range. Generally, the FT-IR spectrum of β-FeOOH shows an intense band at 840 cm^{-1}, two shoulders at 697 and 635 cm^{-1}, and a very intense band at 387 cm^{-1} with a shoulder at 485 cm^{-1} [18]. Weckler and Lutz [19] interpreted two sets of IR vibrations at 847 and 820, and 697 and 644 cm^{-1} in terms of two existing O-H…Cl hydrogen bonds. These chloride ions are located in structural tunnels of the β-FeOOH crystal structure, and it is assumed that they stabilize this structure. Thus the present chloride ions could not have been removed by simple washing. However, with increasing pH (see Table 2) competition occurred between chlorides and hydroxide ions, followed by the dissolution of β-FeOOH and formation of α-Fe_2O_3. Small amounts of the α-Fe_2O_3 phase in sample M5 could not be detected in this FT-IR spectrum. On the other hand, the α-Fe_2O_3

and α-FeOOH phases in samples M6 to M8 are well visible. The FT-IR spectrum of sample M9 (Figure 4B) shows a typical amorphous material feature. Very broad bands of small relative intensity at 577 and 448 cm^{-1} can be attributed to small amounts of the α-Fe_2O_3 phase. Samples M10 to M12 show the IR bands typical of α-FeOOH and α-Fe_2O_3. The spectrum of sample M13 with broad IR bands at 688 and 612 cm^{-1} can be assigned to the β-FeOOH phase. Samples M14 to M16 are in line with XRD and Mössbauer measurements, showing the presence of β-FeOOH and α-Fe_2O_3.

Field Emission Scanning Electron Microscopy

FE SEM images of synthesized samples are shown in Figures 5 and 6. An FE SEM image of sample M1 shows the presence of nanoparticles ~35 nm to ~50 nm which are embedded in an amorphous-like matrix. In line with XRD and ^{57}Fe Mössbauer measurements, these nanoparticles correspond to α-Fe_2O_3 and α-FeOOH, whereas the amorphous-like matrix can be assigned to 2-XRD lines ferrihydrite. The amorphous-like matrix is no more visible in samples M2 to M4, but a small increase in the size of these discrete nanoparticles is noticeable. FE SEM images of sample M5 show the presence of discrete nanoparticles of average size ~35 nm. Samples M6 to M8 show the presence of pseudospherical/rhombohedral and elongated particles in the nanosize range (~100 nm) which can be assigned to the mixture of α-Fe_2O_3 and α-FeOOH particles in line with XRD and ^{57}Fe Mössbauer measurements. The aggregation of these particles is also visible. The FE SEM image of sample M9 is mostly showing an amorphous-like matrix (2-XRD lines ferrihydrite) and α-Fe_2O_3. The presence of very small α-Fe_2O_3 nanoparticles was confirmed by their significantly lower B_{hf} value (50.0 T) as opposed to the B_{hf} value of well-crystallized α-Fe_2O_3 (51.8 T) [20]. An increase in the size of these nanoparticles up to ~100 nm in the series M10 to M12 is observable. FE SEM images of sample M13 show big aggregates of very fine β-FeOOH particles, and in the FE SEM images of samples M14 and M15 additional aggregates of not-so-well-developed shapes are also visible. FE SEM image of sample M15 reveals few cubes, which is in line with XRD analysis since hematite commonly forms cubic particles. However, the FE SEM image of sample M16 showed well-crystallized particles with a shape that resembles a pear or

onion. These onion-like or pear-like particles consist of two parts (ellipsoidal and needle part). These two parts can be found connected as a whole unit or can be found as separated pieces (because some onion-like particles are halved).

Energy-dispersive X-ray spectroscopy

HMTA in synthesis presented in this work has two functions. Firstly, it influences hydrolysis so that fine particles could be obtained (as seen from FE SEM images). The second function is to increase pH value so that Cr^{3+} cations can precipitate, forming solid solutions with iron oxide phases. It is generally known that Cr^{3+} (61.5 pm) makes solid solutions in oxides with Fe^{3+} (64.5 pm) due to very similar radii [13]. Samples autoclaved with Cr^{3+} (M9-M16) were checked with EDS to confirm solid solution formation. EDS spectra were taken for every sample at least three times at different locations and it was found that all samples had 8.77 - 9.60 % of chromium content in relation to iron. Average value of chromium content in relation to iron is 9.73 % for M9, 8.88 % for M10, 8.77 % for M11, 9.06 % for M12, 9.60 % for M13, 9.42 % for M14, 9.50 % for M15 and 9.54 % for M16. These results are showing that most of the chromium used in synthesis is precipitated, forming a solid solution with iron oxide products. It is not excluded that some minor portion of Cr^{3+} is also present in the mother liquor. On the other hand, EDS was also important to confirm Cl^- present in samples. It is mentioned earlier in this article that β-FeOOH has a small quantity of chloride anions present in its structural tunnels (not all chloride anions can be removed in the washing process). EDS can be a useful tool for β-FeOOH phase confirmation if two conditions are met. Firstly, there needs to be enough β-FeOOH content in a sample. If it is present in very small amounts, chloride will not be detected. Secondly, all samples need to be washed very well, so that all chloride that can be washed is removed. If this is the case, only chloride in β-FeOOH tunnels can remain in the sample at the end of the synthesis process. EDS analysis of samples M9-M16 showed chloride presence only in samples M13-M16, which is in line with phase analysis with XRD and Mössbauer spectroscopy.

Conclusions

In this work HMTA is used as additive in forced hydrolysis to influence the precipitation process. HMTA is gradually decomposing at 160 °C, increasing the pH of the autoclaving solution, causing homogeneous hydrolysis of Fe^{3+} and Cr^{3+} cations. As a result, fine uniform nanoparticles are obtained. Four series of samples were to examine the kinetics of these systems. Influences of cation concentration (0.1M and 0.2M $FeCl_3$) and chromium presence (0 and 10%) on the final products were examined.

The influence of cation concentration revealed that relatively diluted systems (0.1 and 0.09 M $FeCl_3$) showed relatively higher pH_{start} and pH_{final} values (Table 2, systems M1-M4 and M9-M12). These systems contain 2-XRD lines ferrihydrite and α-FeOOH at lower autoclaving times and they gradually transform to α-Fe_2O_3 or more complex mixtures with higher α-Fe_2O_3 content with longer autoclaving time. On the other side, there are two systems (M5-M8 and M13-M16) with higher concentrations (0.2 and 0.18 M $FeCl_3$) which turned out to be more acidic, considering their pH_{start} and pH_{final} values. They mostly contain β-FeOOH as a primary product which then transforms to hematite at a longer autoclaving time. All systems tended to yield α-Fe_2O_3 (most stable phase), but their kinetics is very different since α-Fe_2O_3 is created from different precursors.

The other part of the examination is about the influence of chromium on the final products. The presence of chromium made big differences in autoclaved solutions. Firstly, all transformations from primary products to hematite were inhibited, whether hematite is transforming from 2-XRD lines ferrihydrite (M9-M12) or β-FeOOH (M13-M16). That essentially means that samples prepared after 24 h of autoclaving were not pure, they contained significant content of residues of primary products (2-XRD lines ferrihydrite, α-FeOOH, β-FeOOH). This is seen more clearly when system M1-M4 is compared to M9-M12. More concentrated systems are more complicated since α-FeOOH shows better stability and a tendency to form (M9-M12). EDS results confirm that chromium made solid solutions with iron oxide precipitates. Furthermore, chromium is also a key difference that enabled the formation of onion-like particles.

Onion-like (or pear-like) particles can be found in sample M16 (see FE SEM, Figure 6). These particles consist of a needle part and ellipsoidal part (elongated spheres) connected as a whole unit. Kinetic study of onion-shaped particles showed that the first

step is the formation of β-FeOOH nanoparticles, while the second step involves their dissolution and α-Fe_2O_3 crystallization. Onion-like α-Fe_2O_3 particles can be found after 24 h of autoclaving. It should be noted that after 24 hours of autoclaving, there is residual β-FeOOH present in sample M16 (two quadrupole doublets in Mössbauer spectra). Additional experiments made in our laboratory (not presented in this article) showed that mentioned quadrupole doublets don't disappear even after 72 h of autoclaving. Furthermore, it should be emphasized that onion-shaped particles are Cr-doped α-Fe_2O_3, which is confirmed by EDS (chromium content is 9.54 % in relation to iron). Moreover, from the synthesis shown in this article, it can be concluded that onion-shaped particles cannot be prepared without chromium since the reference sample (prepared without Cr^{3+}) consists of rhombohedral particles. Cation concentration also play an important role in formation of onion-shaped particles, since they cannot be obtained in system with 0.09 M $FeCl_3$ + 0.01 M $CrCl_3$, but forms only in more concentrated system of 0.18 M $FeCl_3$ + 0.02 M $CrCl_3$.

The general conclusion is that the effects of Fe^{3+} concentration and presence of Cr^{3+} in the starting autoclaving solutions with HMTA show big differences if their influence on the final products is examined individually, changing the kinetics and product phases. Characterizations presented in this article show that all samples are composites except samples M4 (α-Fe_2O_3) and M13 (β-FeOOH). Furthermore, when HMTA and Cr^{3+} ions are combined in the same synthesis, onion-like particles could be formed if the right synthesis conditions are met. It should be noted that the results in this article are comparable with the results in our previous work where samples were prepared in the presence of chromium, but without HMTA [21]. In mentioned work chromium cations influenced on the particle morphology, but there was no solid solution formation since final pH values were too low, so Cr^{3+} could not precipitate [13].

Experimental

Materials and methods

Preparation of samples

The chemicals $FeCl_3 \cdot 6H_2O$ and $CrCl_3 \cdot 6H_2O$ were supplied by *Alfa Aesar*® and hexamethylenetetramine (commercial name *urotropin*) was supplied by *Kemika*. These chemicals were used in the preparation of samples. Twice distilled water was prepared in own laboratory. Experimental conditions for the preparation of samples are given in Table 2. The prepared precipitation systems were hydrothermally treated using Teflon-lined, non-stirred pressure vessels (45 mL) produced by *Parr instruments Co*.

The prepared solutions were heated in a DX300 gravity oven (*Yamato*) providing temperature uniformity ±1.9 °C at 100 °C and ±3 °C at 200 °C. After a proper time of autoclaving the precipitation systems were gradually cooled to room temperature. The precipitates were then separated from the mother liquor and subsequently washed with twice distilled water using a high-speed centrifuge (*Labogene* Scanspeed 2236R high-speed centrifuge, max rpm: 22 000). Then the washed precipitates were dried in the laboratory dryer for 24 h (90-110 °C).

Characterization

The samples were characterized with the diffractometer APD 2000 manufactured by *ItalStructures* (G.N.R. S.r.l., Novara, Italy). The instrumental parameters were 40 kV, 30 mA, Ni-β filter and Cu$K\alpha_{1,2}$ (1.5405980 Å). Crystal phases were identified using reference XRD patterns shown in the corresponding figures.

^{57}Fe Mössbauer spectra of selected samples were recorded at 295 K in the transmission mode using instrumentation by *WissEl* (Starnberg, Germany). The geometry of the Mössbauer spectrometer was the same in all measurements. The Mössbauer spectrometer was calibrated with α-Fe. The recorded spectra were evaluated with the MossWinn computer program.

FT-IR spectra were recorded in ATR mode using a Frontier spectrometer manufactured by Perkin Elmer.

The precipitates were also inspected with a thermal field emission scanning electron microscope (FE SEM, model JSM-7000F) manufactured by *Jeol Ltd*. A possible presence of chromium in the precipitates was checked with EDS (INCA 350 by *Oxford Instruments*) linked to the FE SEM.

pH values were measured with a combined pH-electrode and pH-meter (type PHM 26) manufactured by *Radiometer*.

Acknowledgements

This work was supported by the Croatian Science Foundation (Grant No. IP-2016-06-8254).

Data availability

Data presented in this study are available on requirement from corresponding author.

Declaration

Conflict of interest

On behalf of all authors the corresponding author states that there is no conflict of interest.

Figure legends

Figure 1 XRD patterns of samples M1 to M8, recorded at 295 K

Figure 2 XRD patterns of samples M9 to M16, recorded at 295 K

Figure 3 A) ^{57}Fe Mössbauer spectra of samples M1 to M8, recorded at 295 K
B) FT-IR spectra of samples M1 to M8, recorded at 295 K

Figure 4 A) ^{57}Fe Mössbauer spectra of samples M9 to M16, recorded at 295 K
B) FT-IR spectra of samples M9 to M16, recorded at 295 K

Figure 5 FE SEM images of samples M1 to M8

Figure 6 FE SEM images of samples M9 to M16

References

[1] Cornell RM, Schwertmann U (2003) The iron oxides: structure, properties, reactions and uses, 2nd ed., Wiley-VCH GmbH & Co KgaA, Weinheim

[2] Musić S, Ristić M, Krehula S (2013) ^{57}Fe Mössbauer spectroscopy in the investigation of the precipitation of iron oxides. In: Sharma VK, Klingelhöfer G, Nishida T (Eds.), Mössbauer spectroscopy: applications in chemistry, biology and nanotechnology. Wiley, Hoboken, pp. 470-504 https://doi.org/10.1002/9781118714614.

[3] Musić S, Šarić A, Popović S (1997) Effects of urotropin on the formation of β-FeOOH. J Mol Struct 410–411:153–156. https://doi.org/10.1016/S0022-2860(96)09576-2

[4] Šarić A, Nomura K, Popović S, Ljubešić N, Musić S(1998) Effects of urotropin on the chemical and microstructural properties of Fe-oxide powders prepared by the

hydrolysis of aqueous $FeCl_3$ solutions. Mater Chem Phys 52:214–220. https://doi.org/10.1016/S0254-0584(97)02032-4

[5] Šarić A, Musić S, Nomura K, Popović S (1999) FT-IR and ^{57}Fe Mössbauer spectroscopic investigation of oxide phases precipitated from $Fe(NO_3)_3$ solutions. J Mol Struct 480–481:633–636. https://doi.org/10.1016/S0022-2860(98)00829-1

[6] Dolgopolova EA, Ivanova OS, Sharikov FY, Ivanov VK, Baranchikov AE, Shcherbakov AB, Trietyakov YD (2012) Microwave-hydrothermal synthesis of gadolinium-doped nanocrystalline ceria in the presence of hexamethylenetetramine. Russ J Inorg Chem 57:1303–1307. https://doi.org/10.1134/S003602361210004X

[7] Wang H, Xie C, Zeng D, Yang Z (2006) Controlled organization of ZnO building blocks into complex nanostructures. J Colloid Interface Sci 297:570–577. https://doi.org/10.1016/j.jcis.2005.10.059

[8] Anas S, Mangalaraja R V., Ananthakumar S (2010) Studies on the evolution of ZnO morphologies in a thermohydrolysis technique and evaluation of their functional properties. J Hazard Mater 175:889–895. https://doi.org/10.1016/j.jhazmat.2009.10.093

[9] Ma G, Salahub S, Montemagno C, Abraham S (2018) Highly active magnesium oxide nano materials for the removal of arsenates and phosphates from aqueous solutions. Nano-Structures and Nano-Objects 13:74–81. https://doi.org/10.1016/j.nanoso.2017.11.006

[10] Collins JL, Lloyd MH, Fellows RL (1987) The Basic Chemistry Involved in the Internal-Gelation Method of Precipitating Uranium as Determined by pH Measurements. Radiochim Acta 42:121–134. https://doi.org/10.1524/ract.1987.42.3.121

[11] Robić M, Ristić M, Krehula S, Jurić M, Musić S (2021) Synthesis of nanocrystalline eskolaite via grimaldiite. Chem Pap. 75:735–741. https://doi.org/10.1007/s11696-020-01338-4

[12] Musić S (1986) Sorption of chromium (VI) and chromium (III) on aluminium hydroxide. J Radioanal. Nucl. Chem. 100:185-196.

[13]Shannon RD (1976) Revised effective ionic radii and systematic studies of

interatomie distances in halides and chaleogenides. Acta Cryst A 32, 751-767. https://doi.org/10.1107/S0567739476001551

[14]Ristić M, De Grave E, Musić S, Popović S, Orehovec Z (2007) Transformation of low crystalline ferrihydrite to α-Fe_2O_3 in the solid state. J Mol Struct 834–836:454–460. https://doi.org/10.1016/j.molstruc.2006.10.016

[15] Krehula S, Musić S (2008) Influence of aging in an alkaline medium on the microstructural properties of α-FeOOH. J Cryst Growth 310:513–520. https://doi.org/10.1016/j.jcrysgro.2007.10.072

[16] Serna CJ, Ocaña M, Iglesias JE (1987) Optical properties of α-Fe_2O_3 microcrystals in the infrared. J Phys C Solid State Phys 20:473–484. https://doi.org/10.1088/0022-3719/20/3/017

[17] Wang Y, Muramatsu A, Sugimoto T (1998) FTIR analysis of well-defined α-Fe_2O_3 particles. Colloids Surfaces A Physicochem Eng Asp 134:281–297. https://doi.org/10.1016/S0927-7757(97)00102-7

[18] Žic M, Ristić M, Musić S (2010) The effect of temperature on the crystallization of α-Fe_2O_3 particles from dense β-FeOOH suspensions. Mater Chem Phys 120:160–166. https://doi.org/10.1016/j.matchemphys.2009.10.040

[19] Weckler B, Lutz HD (1998) Lattice vibration spectra. Part XCV. Infrared spectroscopic studies on the iron oxide hydroxides goethite (α), akaganéite (β), lepidocrocite (γ), and feroxyhite (δ). Eur J Solid State Inorg Chem 35:531–544. https://doi.org/10.1016/S0992-4361(99)80017-4

[20] Murad E, Cashion J (2004) Mössbauer Spectroscopy of Environmental Materials and their Industrial Utilization, Kluwer Academic Publishers, Boston, Dordrecht, New York, London

[21] Robić M, Ristić M, Kuzmann E, Homonnay Z, Krehula S, Musić S (2021) Forced hydrolysis of $FeCl_3$ solutions in the presence of Cr^{3+} ions. J. Phys. Chem. Solids 156:110166. https://doi.org/10.1016/j.jpcs.2021.110166

Table 1 Phase identification of the samples as determined by XRD and ^{57}Fe Mössbauer spectroscopy.

	Sample	Autoclaving time / h	Sample composition			
			2-XRD lines ferrihydrite / %	α-FeOOH / %	β-FeOOH / %	α-Fe_2O_3 / %
no chromium (reference system)	M1	2	37.94	22.75	-	39.31
	M2	4	-	29.95	-	70.05
	M3	6	-	22.53	-	77.47
	M4	24	-	-	-	100.0
	M5	2	-	small unknown	96.5	3.50
	M6	4	-	42.81	-	57.19
	M7	6	-	39.58	-	60.42
	M8	24	-	30.16	-	69.84
10 % chromium	M9	2	92.00	-	-	8.00
	M10	4	21.70	11.57	-	66.73
	M11	6	16.11	12.68	-	71.21
	M12	24	11.96	15.62	-	72.42
	M13	2	-	-	100.00	-
	M14	4	-	-	80.54	19.46
	M15	6	-	-	60.53	39.47
	M16	24	-	-	27.64	72.36

Table 2 Experimental conditions for the sample preparation (forced hydrolysis at 160°C)

Sample	Cr / %	[$FeCl_3$] / M	[$CrCl_3$] / M	[HMTA] / M	t / h	pH_{start}	pH_{final}
M1	0	0.1	Ø	0.25	2	3.65	7.19
M2	0	0.1	Ø	0.25	4	3.65	8.54
M3	0	0.1	Ø	0.25	6	3.65	8.95
M4	0	0.1	Ø	0.25	24	3.65	8.95
M5	0	0.2	Ø	0.25	2	2.10	5.23
M6	0	0.2	Ø	0.25	4	2.10	7.48
M7	0	0.2	Ø	0.25	6	2.10	8.08
M8	0	0.2	Ø	0.25	24	2.10	7.82
M9	10	0.09	0.01	0.25	2	2.95	6.67
M10	10	0.09	0.01	0.25	4	2.95	8.94
M11	10	0.09	0.01	0.25	6	2.95	8.91
M12	10	0.09	0.01	0.25	24	2.95	9.20
M13	10	0.18	0.02	0.25	2	1.99	5.33
M14	10	0.18	0.02	0.25	4	1.99	7.30
M15	10	0.18	0.02	0.25	6	1.99	7.20
M16	10	0.18	0.02	0.25	24	1.99	8.03

Table 3 ^{57}Fe Mössbauer parameters of samples M1 to M20 recorded at 295 K.

Sample	Line	δ / mm s^{-1}	Δ or E_q /mm s^{-1}	B_{hf} / T	Γ / mm s^{-1}	Area /%	Phase
M1	M_1*	0.38	-0.20 (f)	50.4	0.27	39.31	H
	M_2*	0.37	-0.25	35.3	0.26	22.75	G
	Q	0.36	0.71		0.59	37.94	FH
M2	M_1*	0.37	-0.19	50.9	0.24	70.05	H
	M_2*	0.36	-0.25	36.4	0.25	29.95	G
M3	M_1*	0.37	-0.19	50.8	0.25	77.47	H
	M_2*	0.36	-0.27	35.9	0.28	22.53	G
M4	M*	0.37	-0.21	50.7	0.24	100.00	H
M5	M	0.37 (f)	-0.20 (f)	51.4	0.31	3.50	H
	Q_1	0.38	0.59		0.36	52.50	A
	Q_2	0.38	1.00		0.44	44.00	A
M6	M_1*	0.37	-0.19	51.3	0.24	57.19	H
	M_2*	0.37	-0.28	36.6	0.22	42.81	G
M7	M_1*	0.37	-0.19	51.4	0.24	60.42	H
	M_2*	0.37	-0.27	37.0	0.22	39.58	G
M8	M_1*	0.37	-0.20	51.4	0.24	69.84	H
	M_2*	0.36	-0.26	36.8	0.22	30.16	G
M9	M*	0.37 (f)	-0.20 (f)	50.0	0.37	8.00	H
	Q	0.36	0.75		0.54	92.00	FH
M10	M_1*	0.37	-0.21	50.7	0.25	66.73	H
	M_2	0.37 (f)	-0.26 (f)	36.8 (f)	0.75 (f)	11.57	G
	Q	0.36	0.70		0.53	21.70	FH
M11	M_1*	0.36	-0.22	50.7	0.26	71.21	H
	M_2	0.37 (f)	-0.26 (f)	36.2	0.90 (f)	12.68	G
	Q	0.35	0.69		0.50	16.11	FH

Table 3 (continue)

Sample	Line	δ / mm s^{-1}	Δ or E_q /mm s^{-1}	B_{hf} / T	Γ / mm s^{-1}	Area /%	Phase
M12	M_1*	0.37	-0.21	50.7	0.26	72.42	H
	M_2	0.37 (f)	-0.26 (f)	36.8 (f)	1.06 (f)	15.62	G
	Q	0.37	0.63		0.55	11.96	FH
M13	Q_1	0.38	0.60		0.32	41.98	A
	Q_2	0.38	0.95		0.46	58.02	A
M14	M*	0.37	-0.21	51.3	0.24	19.46	H
	Q_1	0.38	0.59		0.33	34.35	A
	Q_2	0.37	0.96		0.46	46.19	A
M15	M*	0.37	-0.21	51.4	0.22	39.47	H
	Q_1	0.38	0.60		0.36	30.23	A
	Q_2	0.38	0.99		0.43	30.30	A
M16	M*	0.37	-0.22	51.5	0.24	72.36	H
	Q_1	0.37	0.61		0.30	11.54	A
	Q_2	0.36	0.94		0.48	16.10	A

Key: δ=isomeric shift relative to α-Fe at 295 K, B_{hf}= hyperfine magnetic field, Δ or E_q=quadrupole splitting, Γ=line-width, M=sextet, Q=quadrupole doublet, H=hematite, G=goethite, FH=ferrihydrite, A=akaganeite, (f)=fixed parameters in the fitting process.

Remark: Mössbauer spectra were fitted using the distribution of B_{hf} (*).

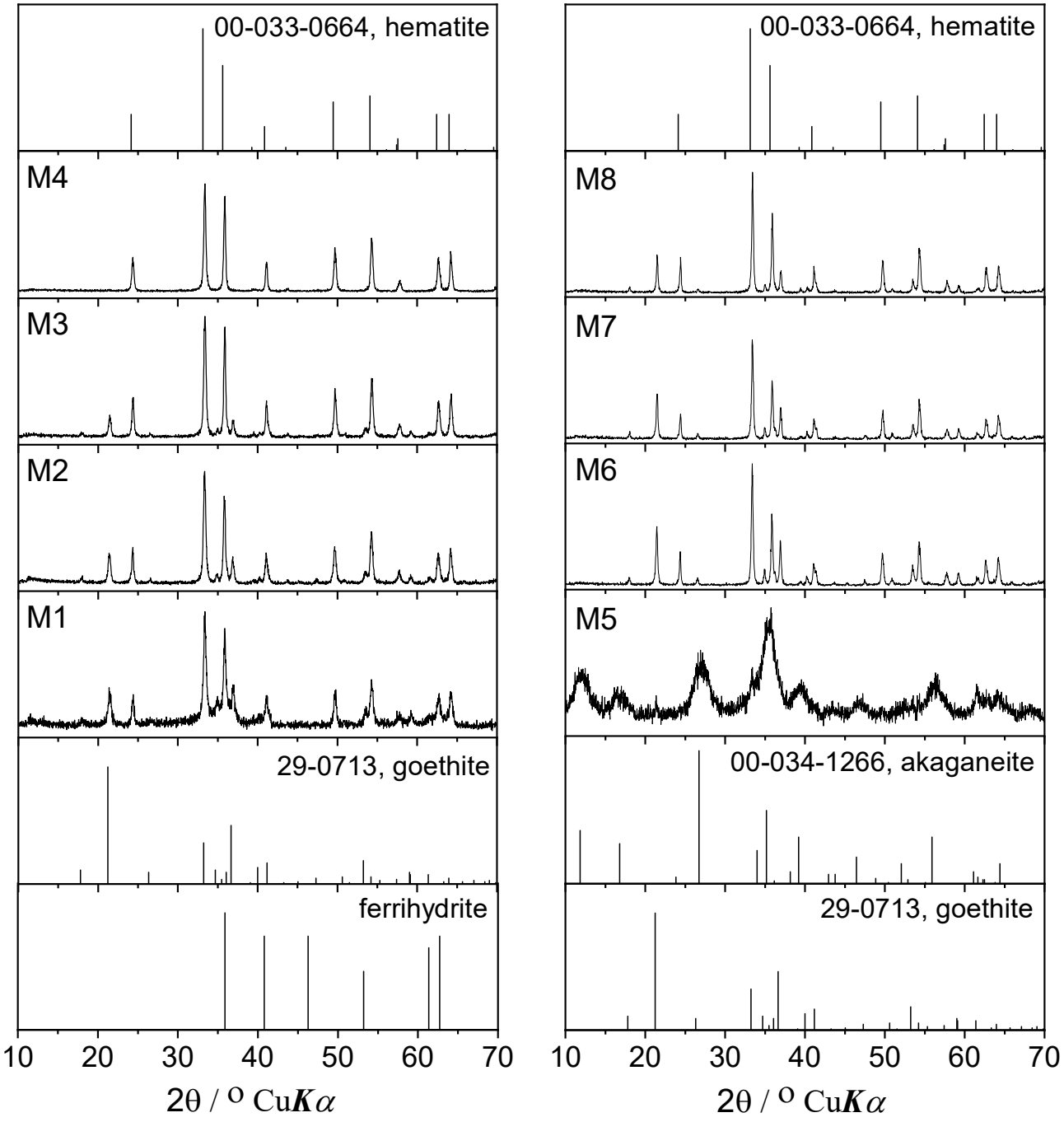
00-033-0664, hematite
M4
M3
M2
M1
29-0713, goethite
ferrihydrite
10
20
30
40
50
60
70
2θ / º Cu**K**α
00-033-0664, hematite
M8
M7
M6
M5
00-034-1266, akaganeite
29-0713, goethite
10
20
30
40
50
60
70
2θ / º Cu**K**α

Fig. 1

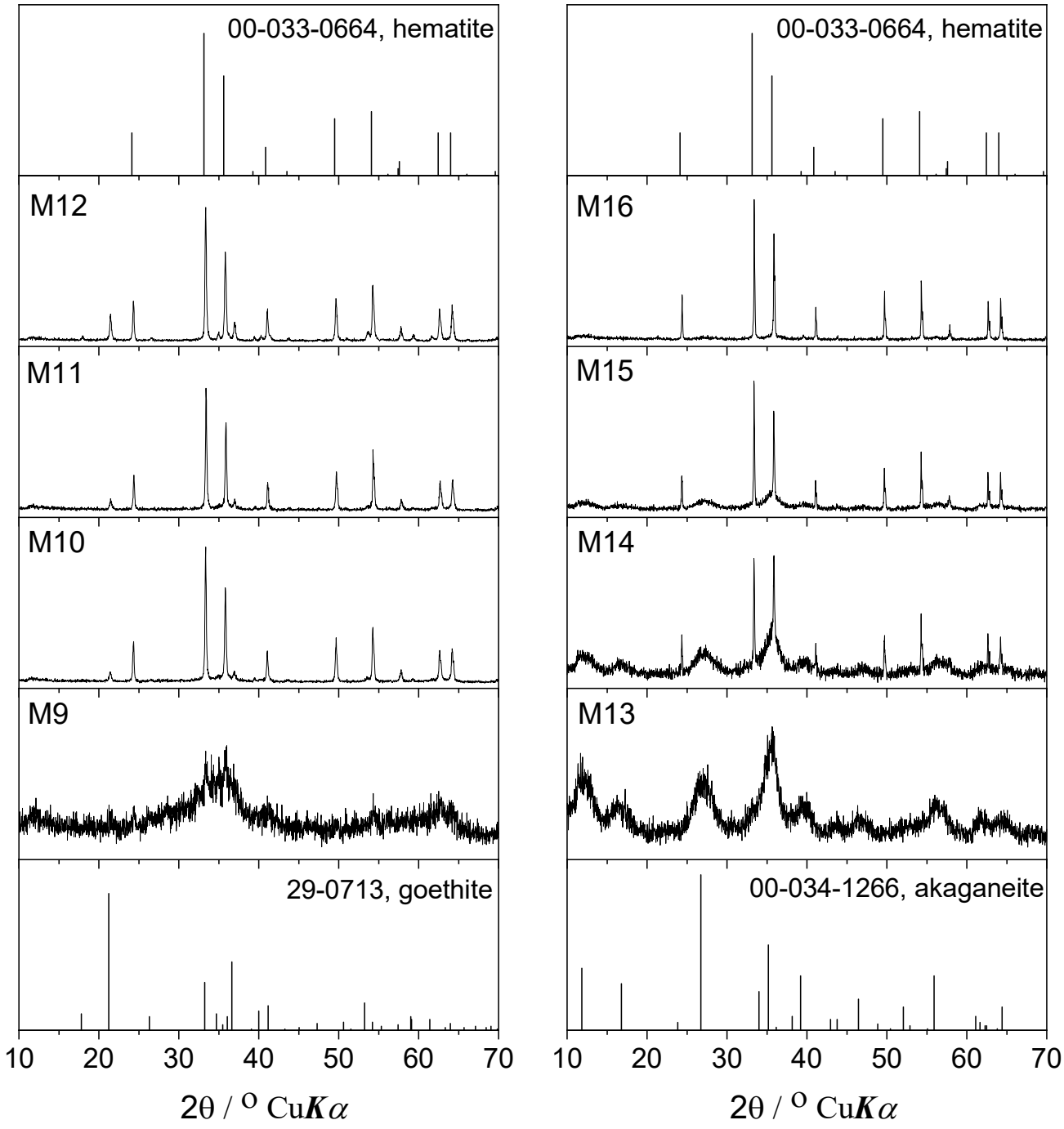
00-033-0664, hematite
M12
M11
M10
M9
29-0713, goethite
00-033-0664, hematite
M16
M15
M14
M13
00-034-1266, akaganeite
10
20
30
40
50
60
70
2θ / ° Cu$K\alpha$
2θ / ° Cu$K\alpha$

Fig. 2

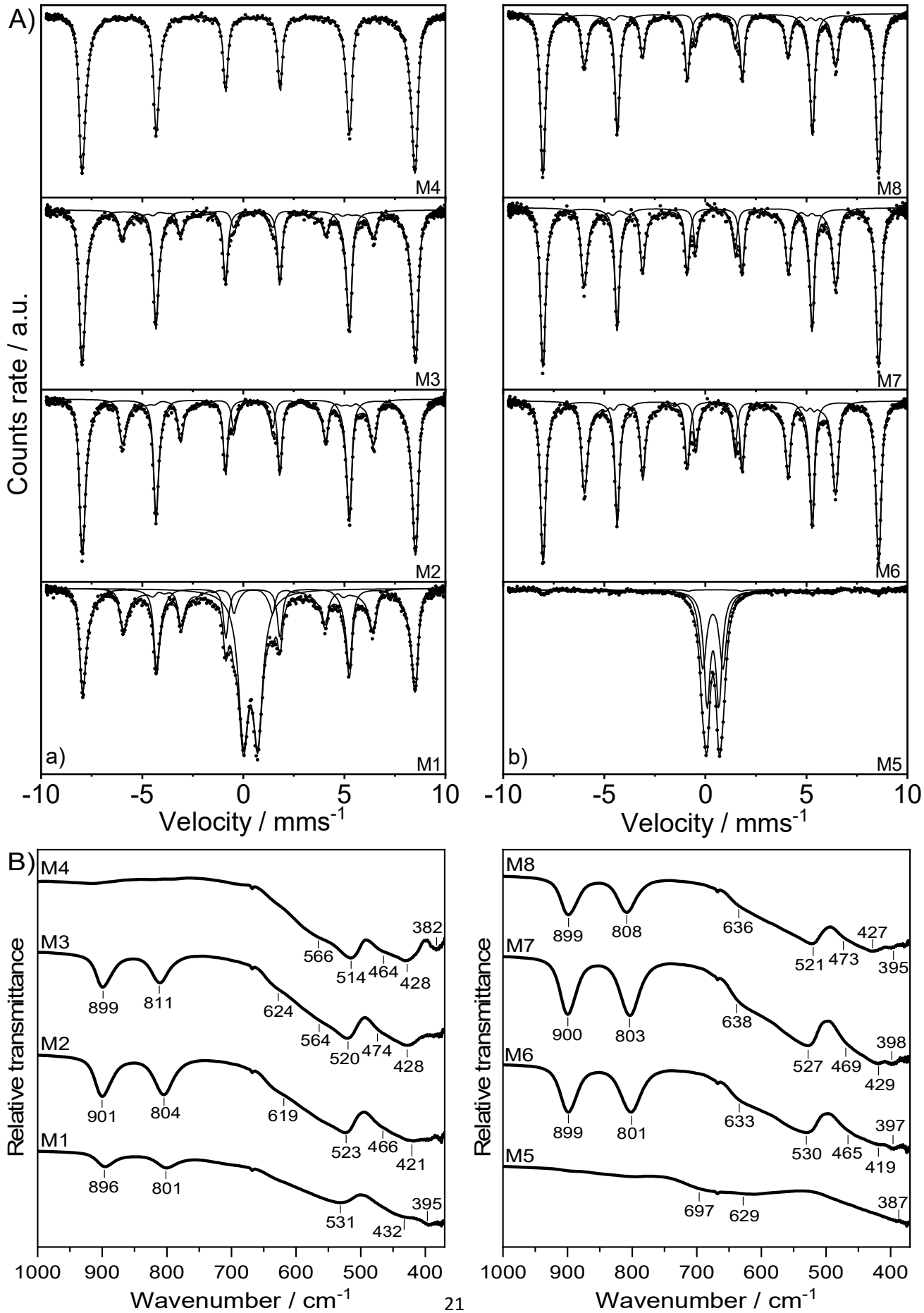
A)
Counts rate / a.u.
M4
M3
M2
M1
a)
M8
M7
M6
M5
b)
-10
-5
0
5
10
Velocity / mms-1
B)
Relative transmittance
M4
382
566
514
464
428
M3
899
811
624
564
520
474
428
M2
901
804
619
523
466
421
M1
896
801
531
432
395
M8
899
808
636
521
473
427
395
M7
900
803
638
527
469
429
398
M6
899
801
633
530
465
419
397
M5
697
629
387
1000
900
800
700
600
500
400
Wavenumber / cm-1

Fig. 3

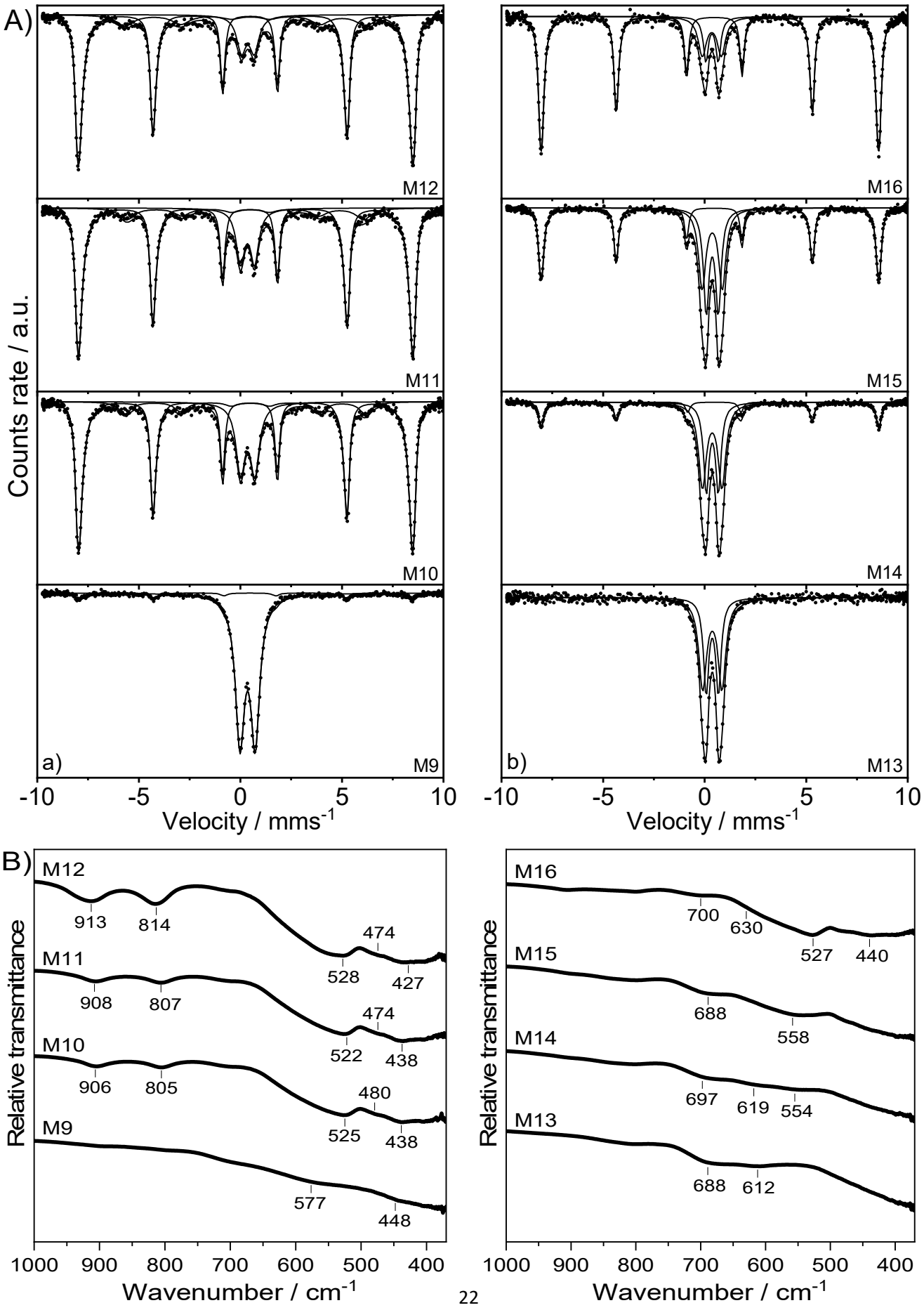
A)
M12
M11
M10
M9
M16
M15
M14
M13
a)
b)
Counts rate / a.u.
-10
-5
0
5
10
Velocity / mms-1
B)
Relative transmittance
913
814
474
528
427
908
807
522
438
906
805
480
525
438
577
448
700
630
527
440
688
558
697
619
554
688
612
1000
900
800
700
600
500
400
Wavenumber / cm-1

Fig. 4

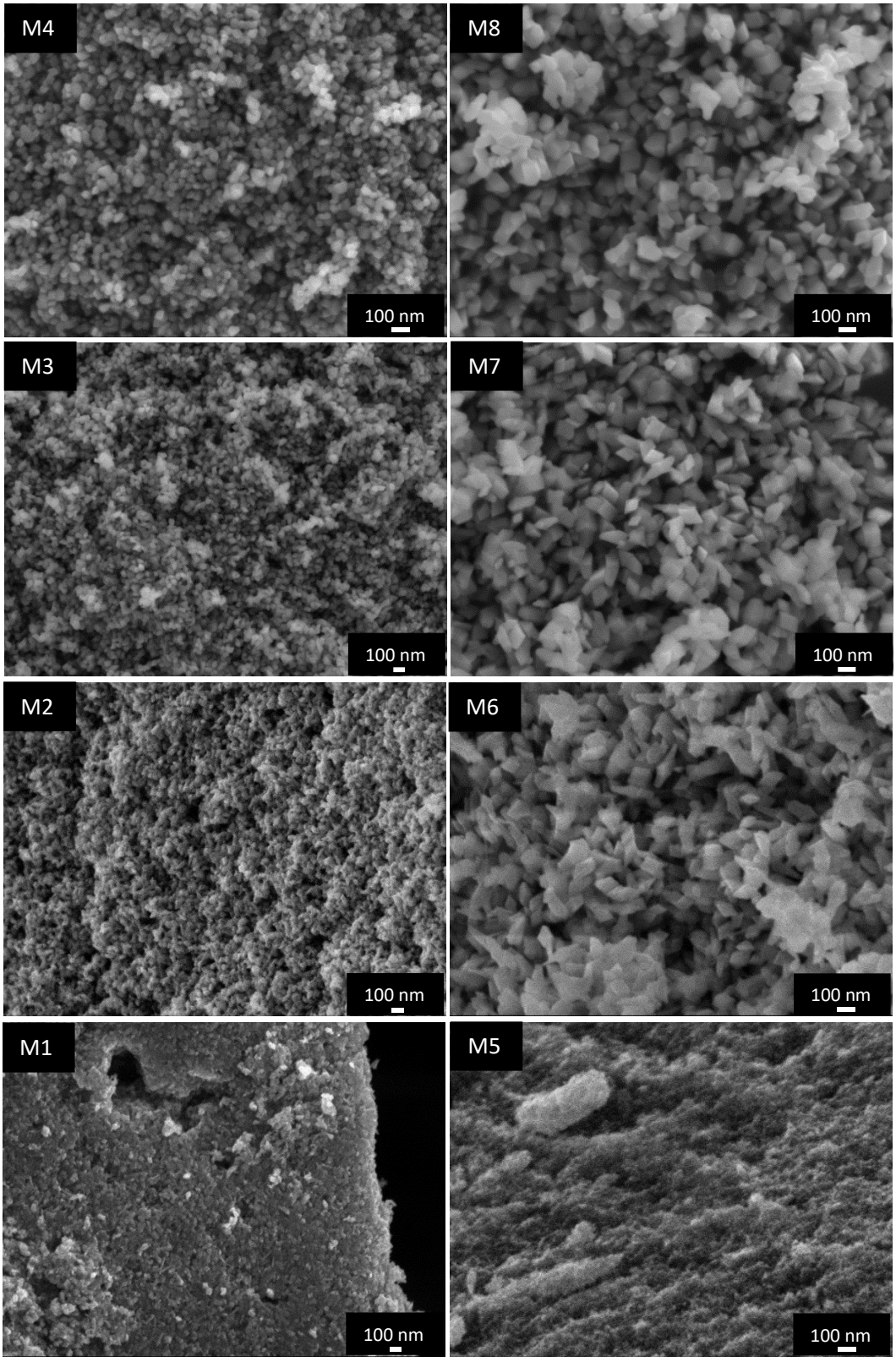
M4
100 nm
M8
100 nm
M3
100 nm
M7
100 nm
M2
100 nm
M6
100 nm
M1
100 nm
M5
100 nm

Fig. 5

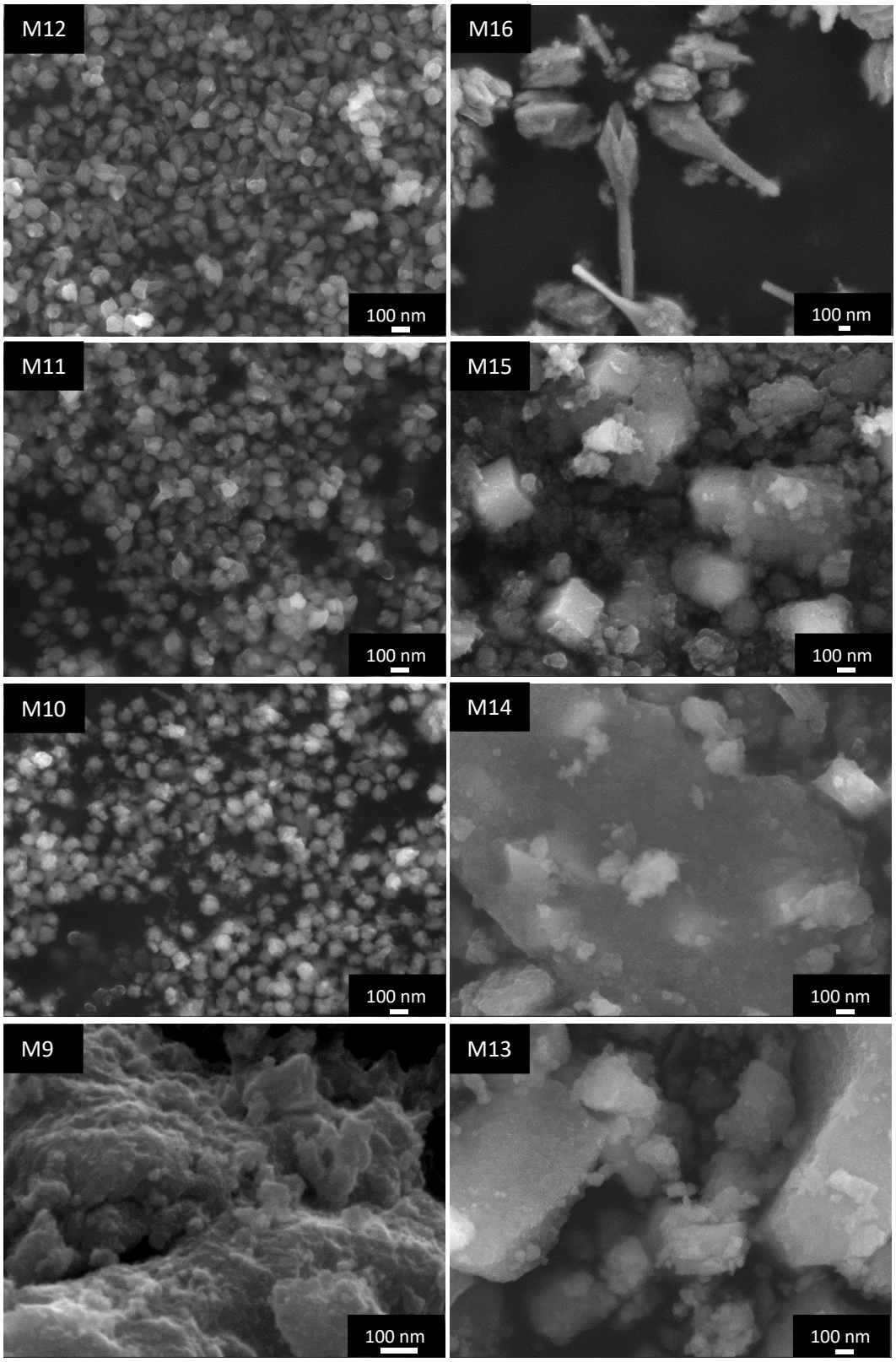
M12
100 nm
M16
100 nm
M11
100 nm
M15
100 nm
M10
100 nm
M14
100 nm
M9
100 nm
M13
100 nm

Fig. 6